JACS
JOURNAL OF THE AMERICAN CHEMICAL SOCIETY
Communication
pubs.acs.org/JACS

Graft-through Synthesis and Assembly of Janus Bottlebrush Polymers from A-*Branch*-B Diblock Macromonomers

Ken Kawamoto,[†,⊥] Mingjiang Zhong,[†,⊥,§] Karim R. Gadelrab,[‡] Li-Chen Cheng,[‡] Caroline A. Ross,[‡] Alfredo Alexander-Katz,[‡] and Jeremiah A. Johnson*[,†]

[†]Department of Chemistry and [‡]Department of Materials Science and Engineering, Massachusetts Institute of Technology, 77 Massachusetts Avenue, Cambridge, Massachusetts 02139, United States

Supporting Information

ABSTRACT: We report the synthesis of Janus bottlebrush block copolymers by graft-through polymerization of branched diblock macromonomers. Self-assembly of the bottlebrushes was characterized by small-angle X-ray scattering, atomic force microscopy, and scanning electron microscopy. Phase separation and packing models of the bottlebrushes were computed, and their self-assembly behavior was corroborated experimentally in bulk and in thin films. Lamellar, hexagonal cylinder, and gyroid phases were observed and modeled. The A-*branch*-B Janus bottlebrush structure provides several unique advantages in the context of bottlebrush polymer assembly, including access to the first examples of gyroid phases.

The merger of advanced polymer architectures with concepts from block copolymer (BCP) assembly[1] offers numerous strategies to control the structure and composition of soft matter on the nanoscale. Several studies investigated the assembly of multiblock linear copolymers, miktoarm star polymers, dendrimers, and bottlebrush BCPs (BBCPs).[2] BBCPs are particularly interesting due to their dense functionality, high molecular weight (MW), lack of entanglement, large molecular size, and tendency to undergo rapid and efficient bulk phase separation.[3]

For BBCP synthesis, graft-through ring-opening metathesis polymerization (ROMP) of norbornene-functionalized macromonomers (MMs) is particularly effective. Grubbs demonstrated the synthesis of various A_n-*block*-B_m BBCPs by sequential addition of "A" and "B" MMs in a graft-through ROMP process (Figure 1a).[4] There are also examples of core−shell BBCPs prepared via graft-through ROMP of norbornene-terminated BCP MMs (Figure 1b).[1b,5]

We are interested in the synthesis of bottlebrush and related nanoarchitectures via graft-through ROMP of branched MMs (BMMs) featuring a polymerizable norbornene group at the center of distinct A and B domains.[6] Such polymers mimic alternating copolymers but are more synthetically accessible.[5] Though there are now several examples of such Janus-type "A-*branch*-B" polymers wherein one of the functional domains is a small molecule, there are relatively few studies wherein A and B are immiscible polymers (Figure 1c).[7]

In contrast to traditional BBCPs (Figure 1a,b), and analogous to random copolymer bottlebrushes,[4a] A and B blocks in A-*branch*-B BBCPs could phase separate with the bottlebrush polymer backbone serving as the interface between the two blocks (Figure 1c).[4b,d,7c,8] This preorganized interface could facilitate assembly and enable access to morphologies that are difficult to achieve, or unknown, for traditional BBCPs.[4b,d,9] Herein, we report the synthesis of such A-*branch*-B BBCPs of varying composition and size. Self-assembly studies confirm that these unique polymer architectures possess advantageous features that could address outstanding challenges in BCP assembly.

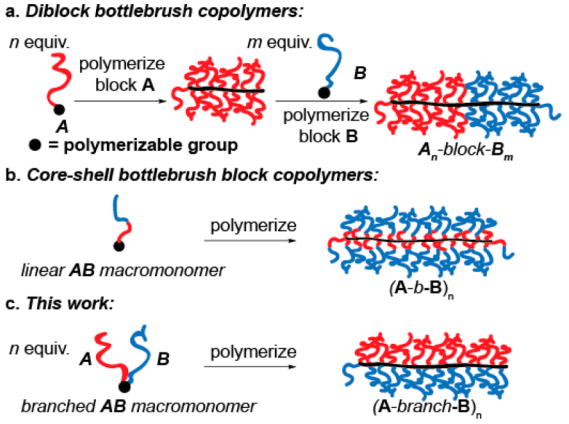

Figure 1. Graft-through polymerization methods for (a) traditional diblock BBCPs, (b) core−shell BBCPs, and (c) A-*branch*-B BBCPs.

We synthesized BMMs with different A and B polymer combinations: (1) polystyrene (PS) and polydimethylsiloxane (PDMS); (2) PDMS and poly(*tert*-butyl acrylate) (P*t*BA); and (3) PS and P*t*BA (Scheme 1; see Synthetic Procedures in SI). Assembly of linear PS-*b*-PDMS has been well-studied;[10] we synthesized eight different variants of BMM **1** with differing number-average MW of PS. These BMMs are referred to as norbornene PS-*x*-*branch*-PDMS-*y*, where *x* and *y* are the MW of PS and PDMS, respectively. ROMP of these BMMs produced A-*branch*-B BBCPs of tunable backbone degree of polymerization (DP).

Structures of thermally annealed samples (145 °C in a vacuum oven for 6 h) of the PS-*branch*-PDMS BMMs and their corresponding BBCPs were studied using small-angle X-ray scattering (SAXS) at 20 °C. In the bulk state, BMMs readily formed ordered lamellar or hexagonal cylinder (HEX)

Received: July 25, 2016
Published: September 1, 2016

ACS Publications © 2016 American Chemical Society

DOI: 10.1021/jacs.6b07670
J. Am. Chem. Soc. 2016, 138, 11501−11504

Scheme 1. Synthesis of BBCPs via ROMP[a]

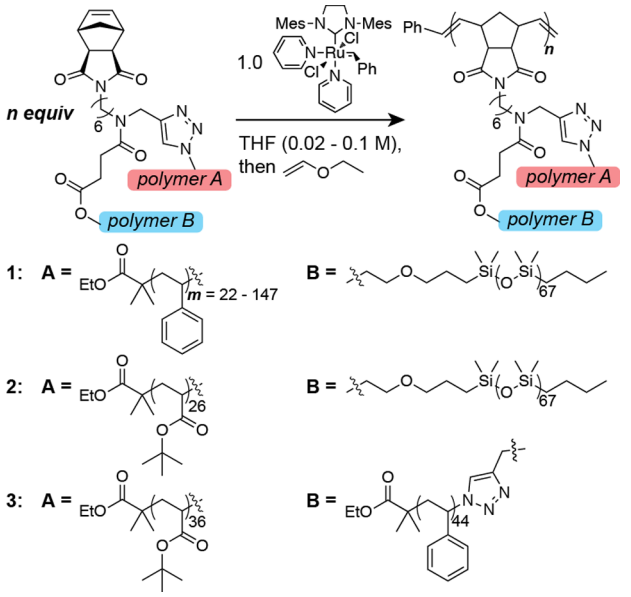

[a](1) **A** = PS, **B** = PDMS; (2) **A** = P*t*BA, **B** = PDMS; (3) **A** = P*t*BA, **B** = PS. Mes = 1,3,5-trimethylbenzene.

morphologies. The resultant BBCPs spanned a wider range of morphologies. The PS-2.3k-*branch*-PDMS-5k BMM formed lamellae with a domain size of 13.0 nm by SAXS, while DP = 10, 20, 30, and 40 BBCPs (0.30 PS volume fraction in all cases) formed highly ordered HEX morphologies with domain sizes of 12.9 or 13.0 nm (Figure 2 and Table S1). Similar behavior was observed for the PS-3.3k-*branch*-PDMS-5k BMM (0.38 PS volume fraction) and its resultant BBCPs (Figure 2). Atomic force microscopy phase images of drop-cast thick films of (PS-3.3k-*branch*-PDMS-5k)$_{25}$ BBCP confirmed the HEX phase (Figure S1). Self-consistent field theory (SCFT) confirmed the HEX morphology at similar PS volume fractions (Figure S2).

For samples made from 4.6k PS and 5k PDMS with nearly equal (0.46:0.54) volume fraction, the BMM and DP = 10, 20, 40, and 80 BBCPs formed lamellae with 14.8, 16.6, 16.6, 16.6, and 16.8 nm domain sizes, respectively. Similar morphological behavior and domain size changes were observed with the BBM and BBCPs synthesized from 6.4k PS and 5k PDMS (0.54 PS volume fraction). SCFT also showed formation of lamellae at this volume fraction (Figure S2).

The small increase in domain spacing for the BBCPs relative to that of BMMs is likely due to the A-*branch*-B BBCP architecture: the confinement of PS and PDMS on the densely grafted backbone stretches the two immiscible chains. When the DP was >10 in this case, we observed little increase in the domain size. Simulation results using SCFT capture this behavior: the close packing of the side chains forces the ends to stretch away from the interface as inferred from the increase of side chain length, L_0, beyond the ideal value of a linear BCP (Figure S3, $L_0^{\text{ideal}} \sim 3.86R_g$, R_g = radius of gyration). Figure S3 depicts the increase of rms end-to-end distance as a function of DP; in the simulations, the effect is prominent until DP ~ 9, after which it plateaus. Equilibrium spacing increased ~45% from $3.37R_g$ (for the BMM) to $4.87R_g$ (at backbone DP = 29).

For BBCPs prepared from PS-8.2k-*branch*-PDMS-5k and PS-9.2k-*branch*-PDMS-5k BMMs, we observed a coexistence of two phases that were indexed to lamellar and gyroidal morphologies. Although phase separation is dominated by the side chains of these polymers, which are quite uniform, this coexistence could arise from the somewhat broad MW distribution for the polymer backbone, especially at higher backbone DP (see SI section IIIA for GPC traces). While the BMM with PS of MW = 8.2k formed ordered lamellar structures, DP = 10, 20, and 40 BBCPs exhibited multiple sets of peaks. Principal and second-order diffraction peaks in the DP = 20 BBCP were indexed to a gyroid morphology, and the third-, fourth-, and fifth-order diffraction

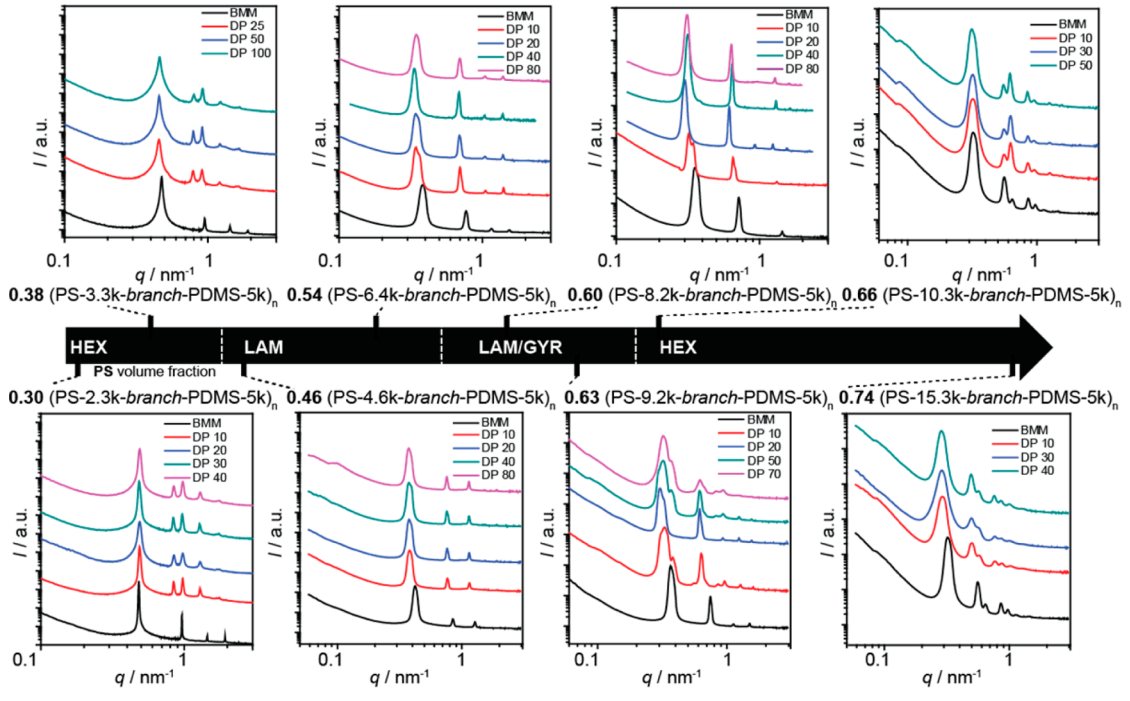

Figure 2. One-dimensional SAXS profiles of PS-*branch*-PDMS BBCPs containing different PS/PDMS volume fractions.

DOI: 10.1021/jacs.6b07670
J. Am. Chem. Soc. 2016, 138, 11501−11504

peaks were indexed to lamellae. BBCPs formed from 9.2k PS appeared to have a greater fraction of gyroid phase.

We also characterized the thin film morphologies of (PS-15.3k-*branch*-PDMS-5k)$_{30}$ (see sample preparation in SI). Well-ordered periodic cylindrical microdomains with 20 nm period and 10 nm line width were obtained for a sample drop-cast from toluene, slowly evaporated for 72 h, and plasma-etched (Figure 3a). Figure 3b shows the annealed thin film morphology of a 28

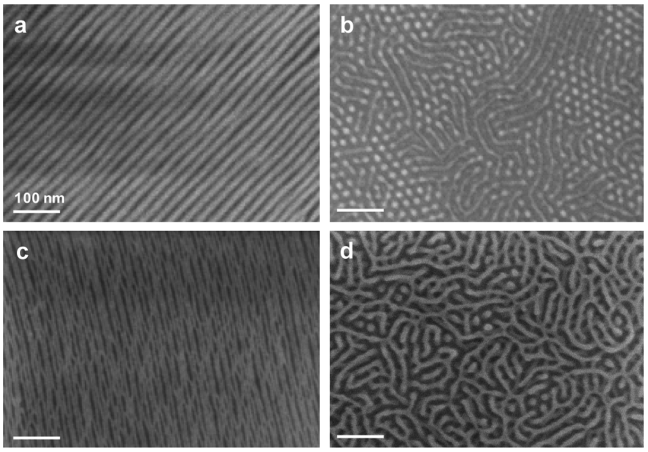

Figure 3. Top-view SEM images of the self-assembled morphology after etching of (a) drop-cast bulk film of (PS-15.3k-*branch*-PDMS-5k)$_{30}$; (b) spin-cast 28 nm thin film; (c) 50 nm film treated with solvent annealing; (d) 50 nm film treated with thermal annealing. Scale bars = 100 nm.

nm as-cast film consisting of cylinders and spheres with average domain spacing of 25 nm. Hole formation suggested that the thickness of the film was insufficient to form a monolayer of microdomains. The structure consists of a wetting layer of PDMS blocks at the substrate and air interface surrounding a layer of PS, with poorly ordered rounded or linear microdomains protruding from the wetting layer. For a 50 nm thick as-cast film, cylindrical microdomains oriented parallel to the substrate were achieved without terrace formation over macroscopic areas (Figure 3c). Each microdomain appeared to be split longitudinally, attributed to oxygen etching of the butyl terminus of the PDMS side chain. In contrast, a thermally annealed 50 nm thick film produced a kinetically trapped state consisting of poorly ordered cylinders or an interpenetrated gyroid-like structure (Figure 3d), with average domain spacing of 20 nm similar to the period of the drop-cast bulk BBCP.

These results indicate that solvent vapor annealing promotes microphase separation with improved ordering compared to thermal annealing. Large χ leads to a high thermodynamic driving force for microphase separation and a high order−disorder transition (ODT) temperature.[11] During solvent vapor annealing, solvent uptake by the film screens the strong interaction between blocks and lowers the diffusion barrier of the polymer chains, enhancing microphase separation kinetics.[12] In contrast to the conventional linear BCP systems with high MW, reduced chain entanglement arising from the steric hindrance between the densely grafted side chains in the BBCP system expedites self-assembly.[13]

We investigated bulk assembly of BMM **2** (Scheme 1), PDMS-5k-*branch*-P*t*BA-3.6k (0.41 P*t*BA volume fraction), which was polymerized to form DP = 25, 50, and 100 BBCPs (see SI). The BMM phase-separated, but only a single peak was observed by SAXS, suggesting limited ordering (Figure 4a). Freshly annealed

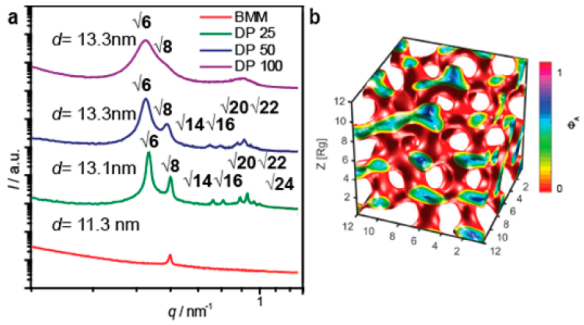

Figure 4. (a) SAXS profiles of PDMS-5k-*branch*-P*t*BA-3.6k BMM and BBCPs. (b) SCFT simulation of A-*branch*-B BBCP gyroid. Color scale represents the density of A blocks. B blocks are transparent for clarity.

BBCPs displayed one broad peak; they could not be indexed to any morphology. After 8 months at ambient conditions, scattering profiles of the DP = 25 and 50 BBCPs became highly ordered. As shown in Figure 4a, the ratio of q_i/q_1, where q_i is the scattering vector at the ith-order diffraction peak, matched that of the gyroid phase ($\sqrt{6}$, $\sqrt{8}$, $\sqrt{14}$, $\sqrt{16}$, $\sqrt{20}$, $\sqrt{22}$, $\sqrt{24}$), where q_1 = 0.481 and 0.472 nm^{-1} for the 25 and 50 unit BBCPs, respectively. The DP = 100 BBCP displayed higher-order peaks but could not be indexed accurately due to the peak broadness. These data represent the first observation of a pure gyroid phase in BBCP assembly, which is made possible by the unique A-*branch*-B BBCP architecture. SCFT simulation of a low χN = 12 A-*branch*-B BBCP recapitulated a bicontinuous gyroid window for f_A = 0.44−0.46 (Figure 4b and SI).

We investigated BMM **3** with PS of MW = 4.6k and P*t*BA of MW = 4.6k and resulting BBCPs. The BMM was disordered, but the SAXS profile of DP = 10 BBCP displayed broad principal and higher-order peaks that were indexed as lamellae (Figure 5a).

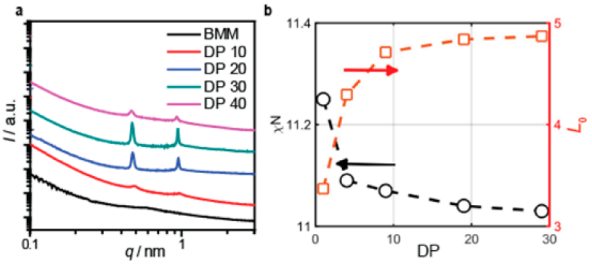

Figure 5. (a) SAXS profiles of PS-4.6k-*branch*-P*t*BA-4.6k BMM and BBCPs. (b) Plot of χN and L_0 vs backbone DP. Increasing backbone DP leads to stretching of the side chains and facilitates phase separation.

SAXS patterns of DP = 20, 30, and 40 BBCPs displayed sharp peaks that were indexed to a lamellar morphology. In this system, we chose BMM components (PS and P*t*BA) to have lower χ than the examples above. The fact that the BMM does not phase separate while the BBCPs do (i.e., the ODT is shifted upon polymerization) suggests that preorganization of the side chains along the dense BBCP backbone reduces the entropic penalty of self-assembly that the BMM suffers.

In SCFT studies, polymerization of the BMM lowers the critical $\chi_{AB}N$ to 11.03 at DP = 29 and leads to stretching of the side chains (increase in L_0), facilitating phase separation. These results suggest that the A-*branch*-B BBCP structure enhances the assembly of short BCPs and could provide access to ultrasmall domains sizes via an architectural approach.[14]

DOI: 10.1021/jacs.6b07670
J. Am. Chem. Soc. 2016, 138, 11501−11504

In conclusion, we demonstrated the synthesis of three novel families of A-*branch*-B BBCPs (PS-*branch*-PDMS, PDMS-*branch*-P*t*BA, and PS-*branch*-P*t*BA) and showed that these polymers have several unique advantages in the context of self-assembly. We observed polymerization-induced changes in bulk morphology and the ODT, as well as gyroid phases. Furthermore, ∼20 nm domain spacing in thin film assemblies from the high MW BBCP breaks the conventional χN limitation.[11] In A-*branch*-B BBCPs with dissimilar side chains, the microdomain period scales with the length of the side chains instead of the overall backbone length. Ultrasmall patterns are fabricated from high MW BBCPs, and the desired pitch of the patterns is controlled by tuning the side chain length. Further process optimization (e.g., commensurate film thickness, annealing process, and plasma etching recipe) is expected to lead to well-ordered self-assembled thin film nanostructures with diverse applications such as nanolithographic pattern transfer. This work should spark interest in exploring the structure and functions of A-*branch*-B bottlebrush block copolymers.

■ ASSOCIATED CONTENT

Supporting Information

The Supporting Information is available free of charge on the ACS Publications website at DOI: 10.1021/jacs.6b07670.

Experimental procedures, AFM images, ^{1}H NMR spectra, GPC traces, simulation details, SAXS data, and synthetic procedures (PDF)

■ AUTHOR INFORMATION

Corresponding Author

*jaj2109@mit.edu

Present Address

§Department of Chemical and Environmental Engineering, Yale University, New Haven, CT 06511.

Author Contributions

⊥K.K. and M.Z. contributed equally.

Notes

The authors declare no competing financial interest.

■ ACKNOWLEDGMENTS

We thank the U.S. Air Force Office of Scientific Research (FA9550-14-1-0292) and the NSF (CHE-1334703) for support. C.A.R. and L.C. acknowledge support of NSF Award DMR1606911. We thank T.M. Swager for GPC. This research used resources of CHESS, which is supported by the NSF and the NIH (Award DMR-1332208), and APS, a U.S. DOE Office of Science User Facility operated for the DOE Office of Science by Argonne National Laboratory (Contract No. DE-AC02-06CH11357). We also thank Dr. Arthur Woll (CHESS) and Dr. Xiaobing Zuo (APS) for their assistance with SAXS. This work made use of Shared Experimental Facilities supported in part by the MRSEC Program of the NSF (Award DMR-1419807).

■ REFERENCES

(1) (a) Bates, F. S.; Fredrickson, G. H. *Phys. Today* **1999**, *52*, 32. (b) Verduzco, R.; Li, X.; Pesek, S. L.; Stein, G. E. *Chem. Soc. Rev.* **2015**, *44*, 2405.

(2) (a) Hawker, C. J.; Frechet, J. M. J. *J. Am. Chem. Soc.* **1990**, *112*, 7638. (b) Frechet, J. M. *Science* **1994**, *263*, 1710. (c) Zheng, W.; Wang, Z.-G. *Macromolecules* **1995**, *28*, 7215. (d) Bohbot-Raviv, Y.; Wang, Z.-G. *Phys. Rev. Lett.* **2000**, *85*, 3428. (e) Gao, H.; Matyjaszewski, K. *Prog. Polym. Sci.* **2009**, *34*, 317. (f) Lutz, J.-F.; Lehn, J.-M.; Meijer, E. W.; Matyjaszewski, K. *Nature Reviews Materials* **2016**, *1*, 16024.

(3) (a) Sheiko, S. S.; Sumerlin, B. S.; Matyjaszewski, K. *Prog. Polym. Sci.* **2008**, *33*, 759. (b) Lee, H.-i.; Pietrasik, J.; Sheiko, S. S.; Matyjaszewski, K. *Prog. Polym. Sci.* **2010**, *35*, 24. (c) Rzayev, J. *ACS Macro Lett.* **2012**, *1*, 1146.

(4) (a) Xia, Y.; Olsen, B. D.; Kornfield, J. A.; Grubbs, R. H. *J. Am. Chem. Soc.* **2009**, *131*, 18525. (b) Xia, Y.; Kornfield, J. A.; Grubbs, R. H. *Macromolecules* **2009**, *42*, 3761. (c) Miyake, G. M.; Piunova, V. A.; Weitekamp, R. A.; Grubbs, R. H. *Angew. Chem., Int. Ed.* **2012**, *51*, 11246. (d) Sveinbjoernsson, B. R.; Weitekamp, R. A.; Miyake, G. M.; Xia, Y.; Atwater, H. A.; Grubbs, R. H. *Proc. Natl. Acad. Sci. U. S. A.* **2012**, *109*, 14332.

(5) (a) Héroguez, V.; Amédro, E.; Grande, D.; Fontanille, M.; Gnanou, Y. *Macromolecules* **2000**, *33*, 7241. (b) Li, Z.; Ma, J.; Lee, N. S.; Wooley, K. L. *J. Am. Chem. Soc.* **2011**, *133*, 1228.

(6) (a) Johnson, J. A.; Lu, Y. Y.; Burts, A. O.; Xia, Y.; Durrell, A. C.; Tirrell, D. A.; Grubbs, R. H. *Macromolecules* **2010**, *43*, 10326. (b) Johnson, J. A.; Lu, Y. Y.; Burts, A. O.; Lim, Y.-H.; Finn, M. G.; Koberstein, J. T.; Turro, N. J.; Tirrell, D. A.; Grubbs, R. H. *J. Am. Chem. Soc.* **2011**, *133*, 559. (c) Liu, J.; Burts, A. O.; Li, Y.; Zhukhovitskiy, A. V.; Ottaviani, M. F.; Turro, N. J.; Johnson, J. A. *J. Am. Chem. Soc.* **2012**, *134*, 16337. (d) Burts, A. O.; Li, Y.; Zhukhovitskiy, A. V.; Patel, P. R.; Grubbs, R. H.; Ottaviani, M. F.; Turro, N. J.; Johnson, J. A. *Macromolecules* **2012**, *45*, 8310. (e) Liao, L.; Liu, J.; Dreaden, E. C.; Morton, S. W.; Shopsowitz, K. E.; Hammond, P. T.; Johnson, J. A. *J. Am. Chem. Soc.* **2014**, *136*, 5896. (f) Sowers, M. A.; McCombs, J. R.; Wang, Y.; Paletta, J. T.; Morton, S. W.; Dreaden, E. C.; Boska, M. D.; Ottaviani, M. F.; Hammond, P. T.; Rajca, A.; Johnson, J. A. *Nat. Commun.* **2014**, *5*, 5460. (g) Mahanthappa, M. K.; Speetjens, F. W. *Block Copolymer Bottlebrushes: New Routes to Ever Smaller Microdomain Sizes*; APS, 2016; 31 pp.

(7) (a) Kale, T. S.; Klaikherd, A.; Popere, B.; Thayumanavan, S. *Langmuir* **2009**, *25*, 9660. (b) Cheng, C.; Yang, N.-L. *Macromolecules* **2010**, *43*, 3153. (c) Li, Y.; Themistou, E.; Zou, J.; Das, B. P.; Tsianou, M.; Cheng, C. *ACS Macro Lett.* **2012**, *1*, 52. (d) Luo, H.; Santos, J. L.; Herrera-Alonso, M. *Chem. Commun.* **2014**, *50*, 536. (e) Burts, A. O.; Gao, A. X.; Johnson, J. A. *Macromol. Rapid Commun.* **2014**, *35*, 168. (f) Rangadurai, P.; Molla, M. R.; Prasad, P.; Caissy, M.; Thayumanavan, S. *J. Am. Chem. Soc.* **2016**, *138*, 7508. (g) Li, H.; Miao, H.; Gao, Y.; Li, H.; Chen, D. *Polym. Chem.* **2016**, *7*, 4476.

(8) (a) Zhao, L.; Byun, M.; Rzayev, J.; Lin, Z. *Macromolecules* **2009**, *42*, 9027. (b) Yuan, Y.-Y.; Du, Q.; Wang, Y.-C.; Wang, J. *Macromolecules* **2010**, *43*, 1739. (c) Li, Y.; Zou, J.; Das, B. P.; Tsianou, M.; Cheng, C. *Macromolecules* **2012**, *45*, 4623. (d) Li, Y.; Christian-Tabak, L.; Fuan, V. L. F.; Zou, J.; Cheng, C. *J. Polym. Sci., Part A: Polym. Chem.* **2014**, *52*, 3250.

(9) (a) Bowden, N. B.; Runge, M. B.; Dutta, S. *PMSE Preprints* **2005**, *92*, 5−6. (b) Theodorakis, P. E.; Paul, W.; Binder, K. *Macromolecules* **2010**, *43*, 5137. (c) Dalsin, S. J.; Rions-Maehren, T. G.; Beam, M. D.; Bates, F. S.; Hillmyer, M. A.; Matsen, M. W. *ACS Nano* **2015**, *9*, 12233.

(10) Jung, Y. S.; Ross, C. A. *Nano Lett.* **2007**, *7*, 2046.

(11) Sinturel, C.; Bates, F. S.; Hillmyer, M. A. *ACS Macro Lett.* **2015**, *4*, 1044.

(12) Jeong, J. W.; Park, W. I.; Kim, M.-J.; Ross, C. A.; Jung, Y. S. *Nano Lett.* **2011**, *11*, 4095.

(13) Rzayev, J. *Macromolecules* **2009**, *42*, 2135.

(14) (a) Bates, C. M.; Seshimo, T.; Maher, M. J.; Durand, W. J.; Cushen, J. D.; Dean, L. M.; Blachut, G.; Ellison, C. J.; Willson, C. G. *Science* **2012**, *338*, 775. (b) Cushen, J. D.; Bates, C. M.; Rausch, E. L.; Dean, L. M.; Zhou, S. X.; Willson, C. G.; Ellison, C. J. *Macromolecules* **2012**, *45*, 8722.